

# Nano-scale fatigue study of LPCVD silicon nitride thin films using a mechanical-amplifier actuator

Wen-Hsien Chuang<sup>1</sup>, Rainer K Fettig<sup>2</sup> and Reza Ghodssi<sup>1</sup>

<sup>1</sup> MEMS Sensors and Actuators Lab (MSAL), Department of Electrical and Computer Engineering and the Institute for Systems Research, University of Maryland, College Park, MD 20742, USA

<sup>2</sup> NASA Goddard Space Flight Center, Greenbelt, MD 20771, USA

Received 22 January 2007, in final form 22 February 2007

Published 4 April 2007

Online at [stacks.iop.org/JMM/17/938](http://stacks.iop.org/JMM/17/938)

## Abstract

This paper describes a nano-scale tensile test to study the fatigue properties of LPCVD silicon nitride thin films using a novel electrostatic actuator design. Mechanical-amplifier devices made in silicon nitride thin films can apply controllable tensile stress (2.0–7.8 GPa) to test structures with relatively low actuation voltages (5.7–35.4  $V_{\text{RMS}}$ ) at the resonant frequencies of the devices. The test devices are fabricated using a surface micromachining technique in combination with deep reactive ion etching and ion milling. With the recently developed experimental techniques inside a focused-ion-beam system, *in situ* fatigue measurements are performed on silicon nitride test structures with beam widths of 200 nm. The silicon nitride test structures are found to exhibit time-delayed failures with continuous increases in their compliance. By reducing the applied tensile stress to 3.8 GPa, the test structures can survive cyclic loadings up to  $10^8$  cycles.

(Some figures in this article are in colour only in the electronic version)

## 1. Introduction

Along with rapid development of microelectronics technologies into the nano-scale regime, fabrication of nanoelectromechanical systems (NEMS) becomes feasible with a similar processing technique. Recently, NEMS have attracted much interest due to their unique capabilities based on different device designs, such as extremely high resonant frequencies, ultra-fine detection resolution, ultra-low power consumption and extremely high mechanical compliance. Current reported applications include VHF (very high frequency) mechanical resonators [1], mechanical electrometers yielding sensitivity below a single electron charge [2], measurement of the quantum of thermal conductance [3] and nanorobots [4]. During the development of NEMS devices, the extremely high surface-to-volume ratios and the unconventional characteristic range of operation have become the critical challenges to realize the full potential of NEMS applications. Since the fundamental material

behaviors on the nano-scale will be dominated by surface and atomistic properties, they may be completely different from the theories for bulk materials.

Understanding mechanical properties of materials on the nano-scale is important for the design of electronic devices and NEMS, as these devices may suffer thermal or mechanical stress during operation. Extensive tests of microelectromechanical system (MEMS) materials have been carried out for evaluating their mechanical properties since 1990 [5–7], though values for some materials are still not available. On the other hand, characterization of mechanical properties on the nano-scale is challenging and the reported data are extremely limited due to difficulties in making nano-scale test specimens and problems associated with measuring ultra-small physical phenomena during experiments. In previous studies, ultra-thin (12–170 nm) single-crystalline silicon cantilevers were fabricated using high-yield processes, and Young's modulus of this thin film was obtained by measuring resonant frequencies of these cantilevers [8]. Due

to experimental setup used in this work, fracture strength and fatigue properties requiring high applied stress are difficult to be tested. Another group reported that nano-scale single-crystal silicon and silicon dioxide doubly clamped beams, with the smallest dimension of 200 nm, were fabricated by field-enhanced anodization with an atomic force microscope (AFM) [9, 10]. Bending tests for these beams were performed using an AFM with a diamond tip mounted on a stainless steel rectangular cantilever to obtain Young's modulus, fracture strength and fatigue properties. This technique utilizes the high-resolution capability of an AFM in combination with a laser reflection setup to measure the deflection of the bent stainless steel cantilever. However, preparation of the test specimens using this technique is only suitable for single-crystal silicon and silicon dioxide, and the high fracture strength of nano-scale thin films may introduce significant deformation on the diamond tip, which is not considered in their analytic model. Furthermore, the slow actuation speed of the AFM tip used in their setup makes high-cycle fatigue study difficult.

This work presents a new test device to study the fatigue properties of nano-scale silicon nitride thin films. Mechanical amplification of the test device is achieved based on a resonant technique to obtain different stress levels without high applied voltages. All experiments are performed inside a focused-ion-beam (FIB) system with a previously developed measurement setup [11]. The presented device design, fabrication processes and experimental techniques are suitable for characterizing fatigue properties of a number of NEMS materials and can be extended for different NEMS/MEMS applications.

## 2. Device design

In our previous study [12], a novel electrostatic actuator was designed and fabricated to study the fatigue properties of a microshutter array, a programmable field selector inside NASA's James Webb Space Telescope [13–15], on the micro-scale. The challenge facing the design of this electrostatic actuator is to obtain high and controllable torsional operating stress via a fixed gap. If the gap between two electrodes is increased, the required amplitude of the applied voltage becomes extremely high to actuate this device. On the other hand, if the gap is small, there is not enough room for movement to introduce high stress levels to structures. To solve this limitation, we separate the location for applying electrostatic energy with the location for creating physical movement in this device, and utilize the maximum response in a physical system at its resonant frequency.

Based on the same design principles, the mechanical-amplifier (MA) actuator used in this study is shown in figure 1. Two resonators are connected serially with two common *torsion bars* to solve the limitation of small displacement amplitude with electrostatic actuation at low applied voltages. During operation, two ac voltages (sinusoidal waveforms) with a 90° phase difference are applied to resonator 1, causing the blades of resonator 1 move up and down alternately. The applied electrostatic energy is transferred to resonator 2 via the common torsion bars. The vibration of resonator 2 is then amplified by its quality factor when the frequency of pumped energy matches its resonant frequency. According to this operation principle, the vibration

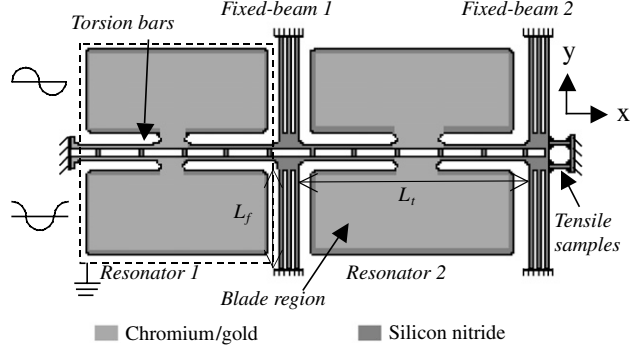


**Figure 1.** Schematic diagram of a mechanical-amplifier actuator. The rectangle (dashed line) represents a ground electrode.

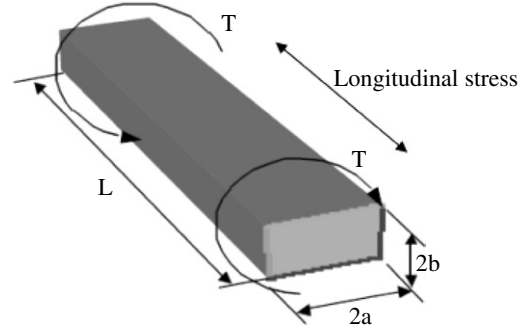


**Figure 2.** A rectangular torsion bar subjected to a pure torque  $T$ . There is longitudinal stress in the torsion bar during twisted motion.

amplification and amplitude of resonator 2 can be controlled by the frequency and amplitude of the input electrostatic energy, respectively. In order to prevent non-torsional movement on torsion bars without significant energy loss during operation, fixed-beam 1 (three suspended beams) is utilized to increase lateral stiffness.

The purpose of the dual-bar configuration used in this device is to increase axial stress while reducing the rotational stiffness. Consider a torsion bar subjected to a pure torque  $T$  as shown in figure 2. In addition to shear stress, it has been proven that there are also longitudinal stress in the torsion bar and a stress component normal to the axis of rotation, which increases the torsional resistance and causes a ‘stiffening’ effect [16]. The maximum shear stress  $\tau_{\max}$ , the maximum tensile stress  $\sigma_t$ , and the total applied torque  $T$  for a twisted bar can be expressed as [16]

$$\tau_{\max} = \frac{3T}{8ab^2} \left[ 1 + 0.6095 \frac{b}{a} + 0.8865 \left( \frac{b}{a} \right)^2 - 1.8023 \left( \frac{b}{a} \right)^3 + \left( \frac{b}{a} \right)^4 \right] \quad (1)$$

$$\sigma_t = \frac{E \tau_{\max}}{12G^2} \left( \frac{a}{b} \right)^2 \quad (2)$$

$$T = KG \frac{\theta}{L} + \frac{8}{45} E \left( \frac{\theta}{L} \right)^3 ba^5, \quad (3)$$

where  $a$  is half the long edge of the rectangular section,  $b$  is half the short edge,  $E$  is Young's modulus,  $G$  is the modulus of rigidity,  $L$  is the length of the torsion bar and  $\theta$  is the

**Table 1.** Dimensions of mechanical-amplifier actuators for nano-scale tensile tests.

Torsion bar ( $\mu\text{m}$ )		Blade region ( $\mu\text{m}$ )		Neck region ( $\mu\text{m}$ )		Fixed-beams 1 and 2 ( $\mu\text{m}$ )		Tensile sample ( $\mu\text{m}$ )		Thickness ( $\mu\text{m}$ )
$L_t$	$W_t$	$L_b$	$W_b$	$L_n$	$W_n$	$L_f$	$W_f$	$L_s$	$W_s$	$T$
108	2	95	35	25	4	40.5	0.8	8	0.2	0.5

twist angle. In these equations,  $K$  is a factor representing the effective polar moment of inertia. The first term on the right side of (3) represents the applied torque  $T$  resisted by torsional shear stress and the second term represents the resistance by tensile stress. It can be seen that the stiffening effect due to the existence of tensile stress is negligible for a small twist angle, but increases rapidly as  $\theta/L$  increases. The maximum tensile stress  $\sigma_t$  of the torsion bar is found to increase with a larger dimension in width (i.e.  $a$  in (2)) for a given torque  $T$ . However, a larger width also increases rotational stiffness significantly due to the higher values of  $K$  and  $a$  on the right side of (3) and leads to a small twist angle  $\theta$ , which is difficult to measure during experiments.

To increase the maximum tensile stress  $\sigma_t$  of the torsion bar and the twist angle  $\theta$  simultaneously, the dual-bar configuration is utilized as shown previously in figure 1. The two torsion bars are connected parallel via small cross-members. The width and the length of each cross-member are  $2 \mu\text{m}$  and  $4 \mu\text{m}$ , respectively, with a separation distance of  $17 \mu\text{m}$ . This configuration increases the effective value of  $a$  in (2), while reducing the effective rotational stiffness since there is less material between these torsion bars to be twisted.

The function of fixed-beam 2 is a mechanical filter to filter out torsional stress; therefore, only tensile stress is applied to *tensile samples* as shown in figure 1. The design principle of this component is to increase the rotational stiffness for twisted motion but lower the longitudinal stiffness (in the  $x$ -direction) for tensile stress. The rotational stiffness of fixed-beam 2 is complicated since the motion of fixed-beam 2 is a combination of elongation/contraction (in the  $y$ -direction) and bending movement during the twist of torsion bars. Even so, the performance of fixed-beam 2 can be evaluated by assuming that most of the rotational stiffness is from the elongation/contraction of the fixed beams and expressed as

$$\frac{K_{\text{tensile}}}{K_{\text{rotational}}} \approx \frac{W_f^2}{4L_f^2}, \quad (4)$$

where  $K_{\text{tensile}}$  is the longitudinal stiffness,  $K_{\text{rotational}}$  is the rotational stiffness,  $W_f$  is the width of fixed-beam 2 and  $L_f$  is the length of fixed-beam 2. The ratio of (4) can be found to be much less than 1 with the dimensions of the mechanical-amplifier actuator presented in table 1. Therefore, the torsional component can be largely filtered out with fixed-beam 2, and only tensile stress is applied to *tensile samples*.

### 3. Fabrication

Fabrication of the mechanical-amplifier actuators begins with a thin silicon wafer ( $250 \mu\text{m}$ ) coated with  $0.5 \mu\text{m}$  thermal oxide and  $0.5 \mu\text{m}$  low-stress LPCVD silicon nitride. A layer of  $50 \text{ \AA}$  chromium and a layer of  $500 \text{ \AA}$  gold are deposited and patterned using a sputtering system and wet etching, respectively, to form the electrodes on resonator 1.

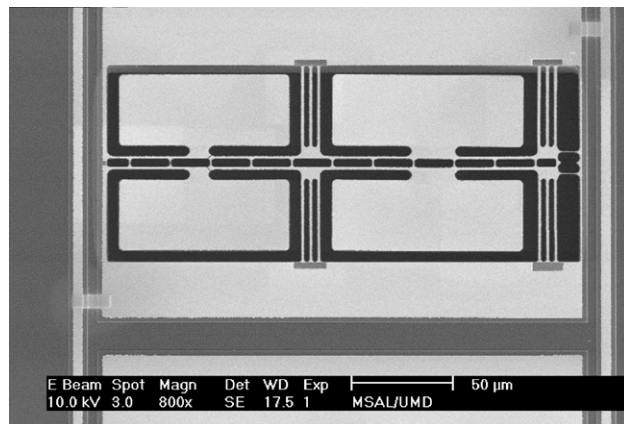


**Figure 3.** Micrograph of a mechanical-amplifier actuator for nano-scale tensile tests after fabrication.

Device structures are then defined on the silicon nitride thin film using reactive ion etching (RIE). Front-to-back alignment is performed to define open windows for further etching processes on the backside of the wafer. Silicon nitride and thermal oxide in the open windows on the backside are removed by RIE and buffered oxide etch, respectively. The silicon substrate is etched through the open windows using deep reactive ion etching (DRIE). The small thickness of silicon wafers used in this experiment provides a more accurate etch profile control, using the thermal oxide as an etch stop layer during the DRIE process.

After microfabrication, a nanomachining step is carried out using a FIB system to adjust the stiffness of fixed-beam 2 (by milling away suspended beams) and the width of *tensile samples* from  $2 \mu\text{m}$  to  $200 \text{ nm}$ . The ion-beam current used in the milling process is  $11 \text{ pA}$  with a nominal spot size of  $15 \text{ nm}$ . The milling depth is  $0.5 \mu\text{m}$ . The fabricated mechanical-amplifier actuator is shown in figure 3 and a close view of a tensile sample is shown in figure 4.

### 4. Experimental techniques

In our previous work, a measurement setup was designed and installed inside a FIB system to characterize Young's modulus and fracture strength of LPCVD silicon nitride thin films at room and cryogenic temperatures [11, 17]. The FEI 620 FIB used in our experiment is a dual beam system, with ion and electron columns, permitting ion milling and *in situ* scanning electron microscopy (SEM). This system also has the ability to deposit platinum (Pt) by ion-induced metal-organic-chemical-vapor deposition (MOCVD).

As shown in figure 1, a ground electrode above the electrodes of resonator 1 is required to actuate the mechanical-amplifier device. In our experiments, a micro-needle inside the measurement setup is utilized as the ground electrode. Here,

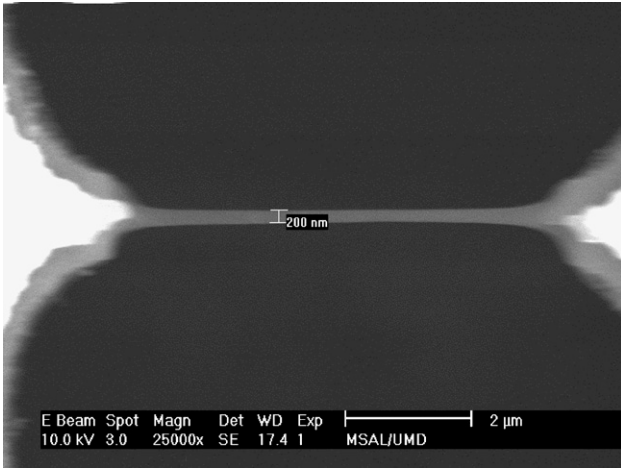


**Figure 4.** Close view of a tensile sample with a width and thickness of 200 nm and 0.5  $\mu\text{m}$ , respectively, after ion milling. The milling current is 11 pA with a nominal spot size of 15 nm.

we describe briefly the formation of the micro-needle ground electrode; further details can be found in [12]. The micro-needle, mounted on a lead–zirconate–titanate (PZT) translator and three stepper motors, is first positioned to contact a silicon nitride membrane coated with a chromium/gold layer. This needle is then welded to this membrane using ion-induced Pt deposition. The micro-needle with the membrane is released by milling away the anchor points of the membrane to the substrate to form the ground electrode. The advantages of this method are (1) the freedom to move the ground electrode and (2) a simplified fabrication process for the mechanical-amplifier device without integrating a ground electrode.

In the FIB system, an SEM image is formed by collecting the secondary electron signal when a fine electron beam is scanned over the surface of a specimen. The collected secondary electron signal varies with the topography and composition of the specimen. This principle can be applied to measure vibrating frequencies of a mechanical-amplifier device. Instead of scanning over the whole surface, a point electron beam is placed in a fixed position where the vibrating blade of a mechanical-amplifier device moves in and out of the electron beam path. This modulates the secondary electron signal with the frequency of vibration, and this signal is acquired with an oscilloscope to determine the vibrating frequency. The mechanism of the vibration frequency determination inside the FIB system is shown in figure 5 [12].

When testing a mechanical-amplifier actuator, the micro-needle ground electrode is positioned above resonator 1 with an approximate height of 5–8  $\mu\text{m}$  and connected to electrical ground. Electrostatic energy is pumped to resonator 1 with two applied ac voltages. The pumped electrostatic energy is then transferred to resonator 2 via common *torsion bars* and drives it at its first resonant mode. The first resonant mode is determined by sweeping a range of frequencies around the expected value and monitoring the vibrating amplitude of resonator 2. Once the resonant mode is obtained, the device is excited at this frequency with a fixed input voltage amplitude for a set period of time. Afterwards, the frequency response is again evaluated by sweeping around the excitation frequency.

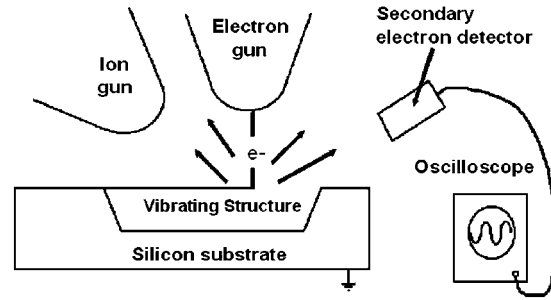


**Figure 5.** Schematic diagram of the mechanism for vibration frequency determination [12].

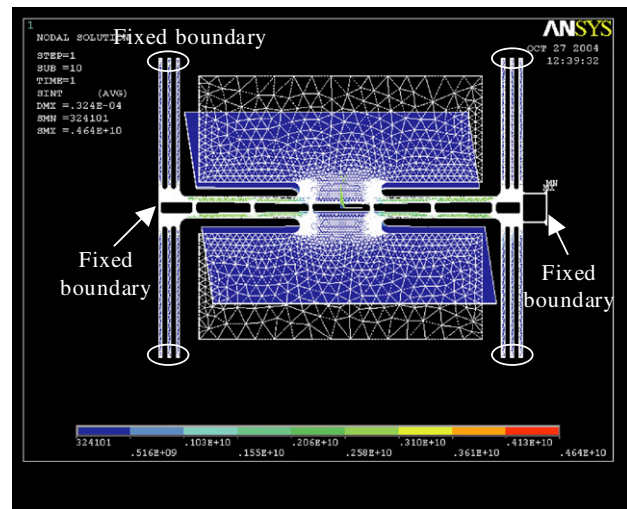


**Figure 6.** ANSYS FEA model used to determine maximum stress on tensile samples. The circles in this figure represent a fixed boundary.

Over time, this allows for the measurement of any change in resonant frequency due to the accumulation of fatigue damage. Given the well-established properties (Young's modulus, Poisson ratio and density) of low-stress LPCVD silicon nitride thin films [17] and the vibrating amplitude of resonator 2 (measured directly using the SEM function), the maximum stress on the structure can be determined from an ANSYS finite-element-analysis (FEA) model. Therefore, the relationship between fatigue life and stress can be obtained.

## 5. Results and discussion

Before testing the mechanical-amplifier actuators, ANSYS FEA models are built to determine the stress distribution on the fabricated tensile samples for different blade displacements as shown in figure 6. In addition, the usage of fixed-beam 2 as a mechanical filter is evaluated. The elements and parameters utilized in these models are presented in table 2. Here, the stress concentration at the ends of *torsion bars* and *tensile samples* are simulated with a radius of curvature  $r = 2.5 \mu\text{m}$ , which is measured using the SEM function provided by the FIB system. Linear and nonlinear analyses, with different mesh sizes, are performed for each data point to verify that there is no geometric effect in these models. Figure 7 presents the maximum operating stress on *tensile samples*

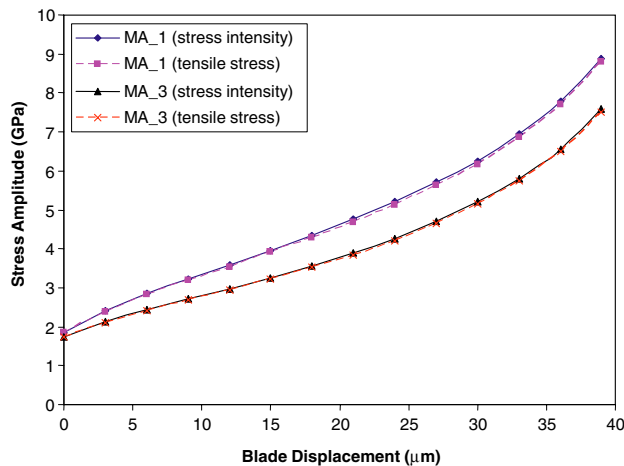


**Figure 7.** Maximum operating stress of the mechanical-amplifier (MA) actuators on tensile samples with different blade displacements from ANSYS FEA models. MA\_1 represents a MA device with one suspended beam as fixed-beam 2 and MA\_3 is a MA device with three suspended beams as fixed-beam 2. Stress intensity in the legend is the total stress applied to the tensile samples, while tensile stress includes only the longitudinal stress.

**Table 2.** Elements and parameters of the mechanical-amplifier actuator utilized in ANSYS FEA models.

Element	Density (kg m <sup>-3</sup> )	Young's modulus (GPa)	Poisson's ratio	Residual stress (MPa)
Solid-92/ solid-187	3000 [19]	260.5 [17]	0.25 [18]	183.4 [18]

for different blade displacements according to these ANSYS models. In figure 7, MA\_1 represents the mechanical-amplifier device with only one suspended beam as fixed-beam 2, while MA\_3 uses three suspended beams as fixed-beam 2. From the simulation results, tensile samples can be considered as structures under only tensile stress, and less than 2% of the stress on these samples is in other directions, even at high stress amplitude. Furthermore, the stress amplitude on tensile samples increases if only one suspended beam is used as fixed-beam 2. One important phenomenon shown in figure 7 is that tensile samples are under longitudinal stress (1.85 GPa) even without any blade displacement. This behavior can be explained by the balance of residual stress/force on asymmetric structures after release [18].

Based on the simulation results, ion milling is performed to remove two suspended beams and keep only one as fixed-beam 2 since this configuration can increase stress amplitude on tensile samples without introducing significant non-tensile components. All devices are tested in a controlled environment (pressure: 10<sup>-6</sup> torr, temperature: 23 ± 1 °C) with input voltages varying from 5.7 V<sub>RMS</sub> to 35.4 V<sub>RMS</sub> using the testing procedure described previously, while the test duration ranges from 3 s to 60 min, or 10<sup>5</sup> to 10<sup>8</sup> cycles. Figure 8 shows a mechanical-amplifier actuator with resonator 2 at its first resonant mode. In this experiment, the input voltage to resonator 1 is 14.1 V<sub>RMS</sub> and the resonant frequency of resonator 2 is found to be 38.09 kHz. The experimental results from the stress-life testing are shown in figure 9. When the maximum operating stress exceeds 4.3 GPa, the mechanical-

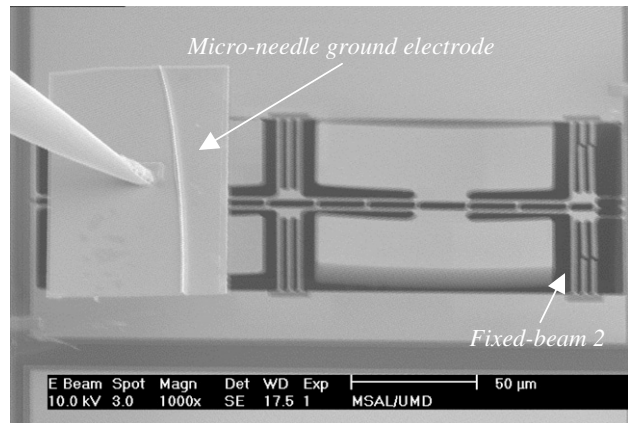


**Figure 8.** Micrograph of a mechanical-amplifier actuator for fatigue tests with resonator 2 at its first resonant mode ( $f_0 = 38.09$  kHz). In this device, only one suspended beam is used as fixed-beam 2.

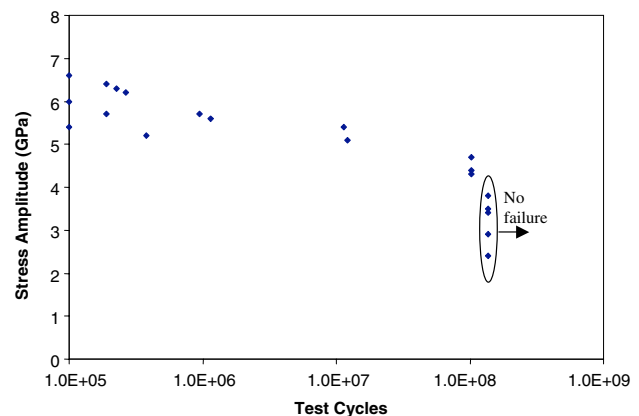


**Figure 9.** Stress-life testing data for nano-scale tensile samples. The circle with a horizontal arrow indicates devices that did not fail under cyclic loading up to 10<sup>8</sup> cycles.

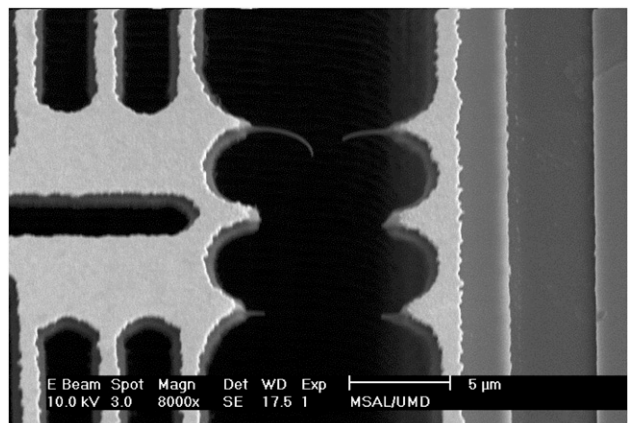


**Figure 10.** Micrograph of tensile samples after cyclic loadings.

amplifier actuators exhibit time-delayed failure. On the other hand, tensile samples with testing stress amplitude below 3.8 GPa survive cyclic loadings beyond 10<sup>8</sup> cycles. An example of broken tensile samples after cyclic loadings is shown in figure 10. A crack initiates at the center of the upper tensile sample. Once the upper tensile sample is broken, all

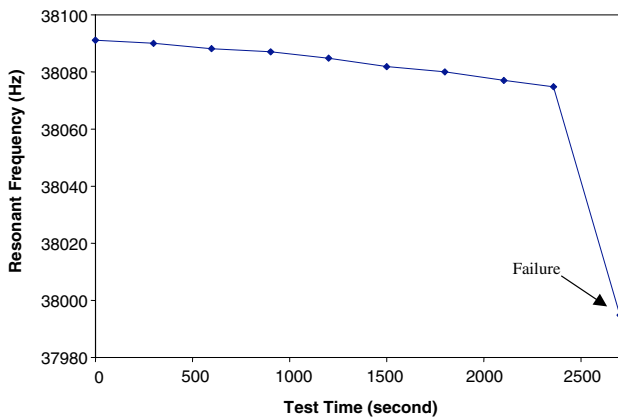


**Figure 11.** Variation of resonant frequency with time for a mechanical-amplifier actuator during fatigue testing (test cycle:  $10^8$  cycles at stress amplitude 4.4 GPa).

axial stress is applied to the lower tensile sample and breaks it immediately. The curl-down broken tensile sample is due to a stress gradient introduced mainly during the ion milling process.

The resonant frequency of the mechanical-amplifier actuator is used to monitor the stiffness of tensile samples during cyclic loadings, and is observed to decrease monotonically with test time as shown in figure 11. The change in resonant frequency indicates that tensile samples become more compliant during the test. This behavior strongly suggests that the failure of tensile samples occurs as a result of the progressive accumulation of damage rather than sudden fracture. In addition, a significant decrease of the resonant frequency is found at the time of failure due to decrease of the effective spring constant of resonator 2 when these tensile samples break.

Several uncertainties may cause errors in the determination of maximum operating stress from ANSYS FEA models. First, the cross sections of tensile samples are not perfectly rectangular due to the ion milling process. The curvature of tensile samples is difficult to measure, especially in the nanometer scale. However, tensile samples are under axial stress during experiments, and irregular sample cross sections do not increase stress concentrations; therefore, the influence of this process imperfection can be neglected. Second, resonator 1 is ignored in the FEA models for simplicity due to its relatively small movement. Third, the applied voltages to the mechanical-amplifier device disturb electron beam signals and cause distortion of scanning electron micrographs. This may introduce errors in the measurements of blade displacements. However, this error can be compensated for by measuring the blade position of a static resonator 2, which operates at a frequency far from its resonant mode with the same applied voltages.

For the testing results, two factors may reduce the fatigue lifetime of the silicon nitride tensile samples in this study. First, nano-scale tensile samples are fabricated using ion milling instead of microfabrication. Damage and gallium implantation on the surfaces and the sidewalls of tensile samples are inevitable. As the surface condition of test structures is a critical factor in inducing premature failure,

the stress-life testing data may not represent the fatigue property of nano-scale silicon nitride thin films fabricated using other methods. Second, the residual stress of the LPCVD silicon nitride ( $\sim 180$  MPa) after deposition induces a 1.85 GPa tensile stress on tensile samples before testing. The existing pre-stress enhances the average stress amplitude and tensile samples do not return to the zero-stress state during experiments. This phenomenon decreases the fatigue resistance of tensile samples. Nonetheless, the stress-life testing results in this study can provide conservative stress amplitude for the reliability design of a nanostructure using silicon nitride thin films in a vacuum environment.

## 6. Conclusions

The paper presents the design, fabrication and testing of a mechanical-amplifier actuator for the fatigue study of nano-scale LPCVD silicon nitride thin films. The design principle is to utilize longitudinal stress produced from two rotated *torsion bars*. The dual-bar configuration used here can increase the longitudinal stress while reducing the rotation stiffness simultaneously. To obtain tensile stress on *tensile samples*, one suspended beam (fixed-beam 2) is connected between the *torsion bars* and *tensile samples*. The high rotational spring constant of this beam can then be used to eliminate the torsional stress. Therefore, only tensile stress is applied to tensile samples, and the amplitude of this stress can be controlled by the frequency and the amplitude of the input electrostatic energy. From the experiments, the mechanical-amplifier actuators exhibit time-delayed failure and the resonant frequencies of these devices decrease monotonically with test time when the maximum operating stress exceeds 4.3 GPa. The change in resonant frequencies indicates that tensile samples become more compliant during the test, and the failure of tensile samples occurs as a result of the progressive accumulation of damage. On the other hand, no fatigue failure of nano-scale LPCVD silicon nitride thin films is found up to  $10^8$  cycles when testing at stress amplitude below 3.8 GPa with a load ratio of 0.48. Further fatigue testing of the mechanical-amplifier actuators fabricated with microfabrication techniques without ion milling damage is under investigation, and the presented test devices and experimental technique can be extended to characterize fatigue properties for other thin film materials.

## References

- [1] Cleland A N and Roukes M L 1996 Fabrication of high frequency nanometer scale mechanical resonators from bulk Si substrates *Appl. Phys. Lett.* **69** 2653
- [2] Cleland A N and Roukes M L 1998 A nanometer-scale mechanical electrometer *Nature* **392** 160
- [3] Schwab K, Henriken E A, Worlock J M and Roukes M L 2000 Measurements of the quantum of thermal conductance *Nature* **404** 974
- [4] Requicha A A G 2003 Nanorobots, NEMS, and nanoassembly *Proc. IEEE* **91** 1922–33
- [5] Muller R S 1990 Microdynamics *Sensors Actuators A* **21** 1–8
- [6] Yi T and Kim C-J 1999 Measurement of mechanical properties for MEMS materials *Meas. Sci. Technol.* **10** 706–16
- [7] Winchester K J and Dell J M 2000 Nano-indentation characterization of PECVD silicon nitride thin films *IEEE Optoelectron. Microelectron. Mater. Dev.* **1** 117–20

- [8] Li X, Ono T, Wang Y and Esashi M 2002 Study of ultra-thin NEMS cantilevers-high yield fabrication and size-effect on Young's modulus of silicon *IEEE Microelectromech. Syst.* **1** 427–30
- [9] Namazu T, Isono Y and Tanaka T 2000 Evaluation of size effect on mechanical properties of single crystal silicon by nanoscale bending test using AFM *J. Microelectromech. Syst.* **9** 450–9
- [10] Sundararajan S and Bhushan B 2002 Development of AFM-based techniques to measure mechanical properties of nanoscale structures *Sensors Actuators A* **101** 338–51
- [11] Chuang W-H, Luger T, Fettig R K and Ghodssi R 2005 A cryogenic measurement setup for microelectromechanical systems used in space applications *Rev. Sci. Instrum.* **76** 045105–1 045105–6
- [12] Chuang W-H, Fettig R K and Ghodssi R 2005 An electrostatic actuator for fatigue testing of low-stress LPCVD silicon nitride thin films *Sensors Actuators A* **121** 557–65
- [13] Moseley H S, Fettig R K, Kuttyrev A, Bowers C, Kimble R, Orloff J and Woodgate B 1999 Programmable 2 dimensional microshutter arrays *Proc. SPIE* **3878** 392–7
- [14] Moseley H S, Fettig R K, Kuttyrev A, Li M, Mott D and Woodgate B 2000 Status of the development of a 128 × 128 microshutter array *Proc. SPIE* **4178** 51–8
- [15] Li M *et al* 2001 Fabrication of microshutter arrays for space application *Proc. SPIE* **4407** 295–303
- [16] Young W C 1989 *Roark's Formulas for Stress and Strain* (New York: McGraw-Hill)
- [17] Chuang W-H, Luger T, Fettig R K and Ghodssi R 2004 Mechanical property characterization of LPCVD silicon nitride thin films at cryogenic temperatures *J. Microelectromech. Syst.* **13** 870–9
- [18] Chuang W-H 2005 MEMS-based silicon nitride thin film materials and devices at cryogenic temperatures for space applications *PhD Thesis* University of Maryland, College Park
- [19] Senturia S D 2001 *Microsystem Design* (Norwell: Kluwer)